A Comprehensive Thermogravimetric Analysis Multifaceted Method for the Exact Determination of the Composition of Multi-functional Metal-Organic Framework Materials

Isabel Abánades Lázaro [a]*

[a] Functional Inorganic Materials Team, Instituto de Ciencia Molecular (ICMol), Universitat de València, Paterna 46980, València, Spain

* E-mail: Isabel.abanades@uv.es; Web: Www.deftimofs.com

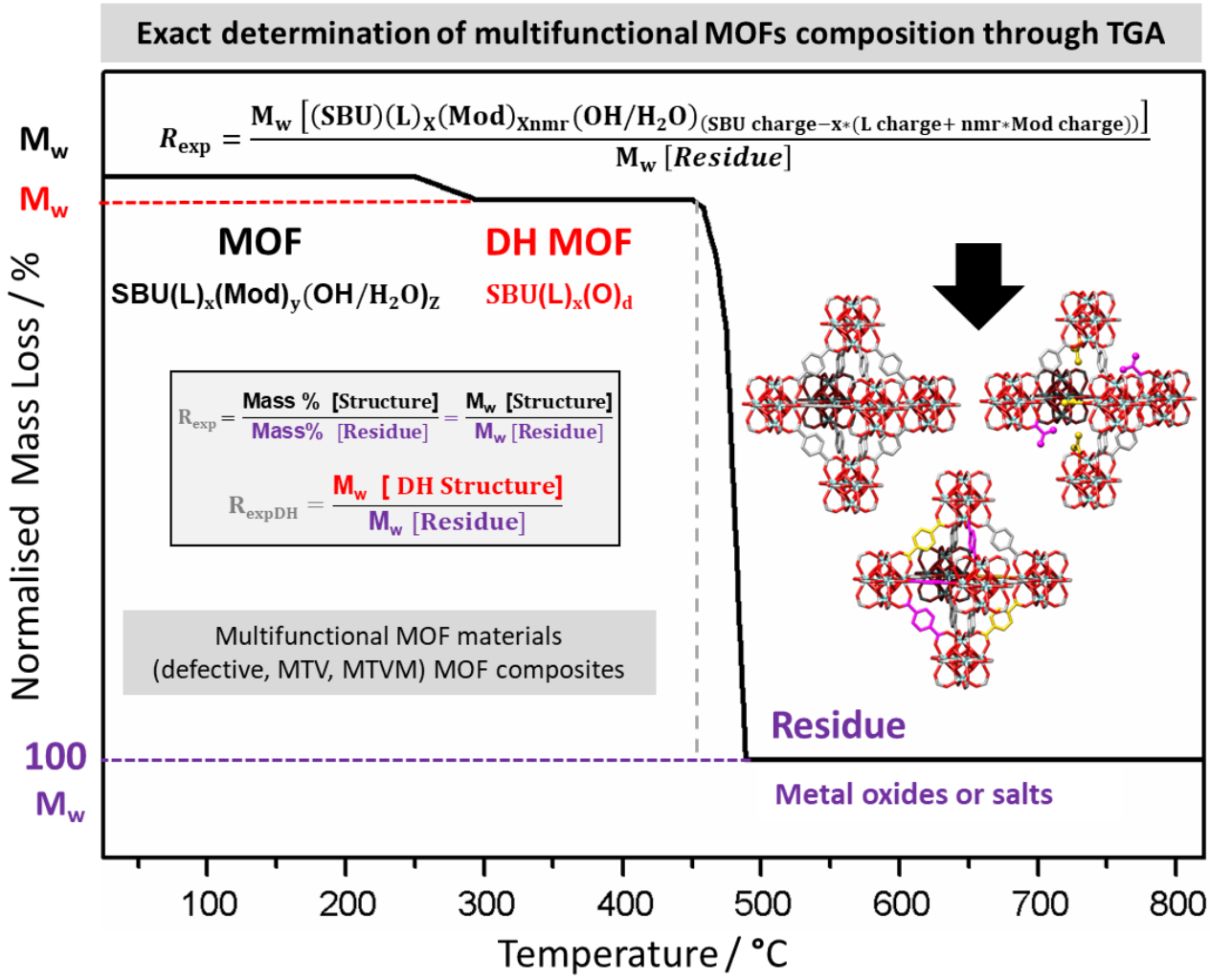

Key Topic: Determination of MOFs' composition through thermal analysis.

Summary: The literature-reported methods to characterise the composition of MOF materials are revised, and a new multi-faceted TGA methodology to determine the exact composition of MOFs is presented. An example applicable to any defective MOF is provided, with specific examples for the most common MOFs. This methodology is applied to multicomponent MOFs, mixtures of MOFs and MOF composites using UiO-66 as an example.

Abstract

Thermogravimetric analysis (TGA) has been widely used as a tool to characterise the composition of materials such as Metal-Organic Frameworks (MOFs). However, given their multifunctionality and structural complexity, examples of detailed methodology for the exact calculation of the composition of complex MOF structures and MOF composites, are lacking in the literature.

Herein, we introduce a new straightforward methodology - based on the experimental ratio between the mass of a structure and its residue - for the exact calculation of the composition of almost any MOF material. We provide a detailed guide for the application of our methodology to different MOF materials, including MOFs in which multiple components fully or partially decompose during the same temperature range as the ligand, and diverse MOF composites, alongside with theoretical calculations demonstrating the exact mathematical determination. The methodology here presented can be also applied to many materials beyond MOFs.

Introduction

Metal-Organic Frameworks (MOFs)[1–4] have garnered a tremendous amount of interest over the past 20 years due to their intrinsic properties such as high thermal and chemical stabilities, high porosity and readily tuneable structure, which have made them attractive for a variety of applications related to porous and/or functional materials.[5–9]

The almost unlimited variety of metal-linker combinations has resulted in a rich landscape of functional materials,[3,10] with ca. 85,000 MOF structures being reported in the Cambridge Crystallographic Data Base as of 2020,[3] whereas some MOFs have only been synthesised as powders, resulting in an even higher number of MOF structures. Their ease of tunability has resulted in the introduction of functionality to the linkers[11] and to the surfaces,[12,13] with efforts being put into the development of accessible post-synthetic,[14] and synthetic surface modification protocols.[15] Due to MOFs' porosity different moieties have been loaded into their pores, such as drugs, metal nanoparticles or catalytical species to name a few, increasing the number of MOF-related structures.[5,10]

The structural complexity and multifunctionality of MOF structures are rapidly evolving as interest in their application increases. The development of multivariate MOFs (MTV MOFs) – frameworks comprised of multiple different linkers – has yielded a range of frameworks demonstrating properties otherwise unobtainable through single linker incorporation.[16–18] Similarly, heterometallic MOFs can have properties absent in the homometallic MOFs.[19,20] Mixed MOF materials have been synthesised sequentially and directly, the first resulting in core-shell MOF on MOFs materials of tuneable properties.[21–23] By combining MOFs with a second material such as silica, metal-oxides, proteins, polymers, cellulose, polyoxometalates, active carbon or graphene oxide among many other possibilities, the performance of MOFs for diverse applications has been enhanced.[24–27]

MOF tailorable chemistry has also increased from the introduction of monotopic modulators to MOF synthesis during a process referred to as coordination modulation.[15] The modulator competes with the linker for the metal nucleation sites[28] and can be attached to the metal clusters of the resultant structure as capping[29] and/or defect-compensating ligands.[30–32] The introduction of multiple modulators to MOFs synthesis - multivariate modulation, MTVM - has also been studied resulting in multifunctional defective structures.[33] Defects often lead to changes in MOFs mechanical and physical properties,[34] porosity[32] and density of open metal sites (chemical reactivity),[35] which are strictly related to applications such as gas storage[36] and catalysis,[37–39] among others.[40–42] However, defects result in non-stoichiometric compositions that hinder the exact determination of MOF structures using common laboratory techniques.[36,43,44]

The performance of MOFs towards diverse applications is related to their composition. However, due to their structural complexity, characterising the exact composition of defective and/or multifunctional MOF structures is challenging.

The use of high-resolution techniques has resulted in an impressive molecular level of visualisation of MOF surfaces and defects,[45–47] providing unaccountable knowledge to the scientific community, but unfortunately, these techniques are still not easily accessible and cannot be used in a day-to-day basis. Thermogravimetric analysis (TGA) is a common laboratory technique that monitors weight changes as a function of temperature and has been used as a tool to quantify the structural composition of materials.[48–54] TGA is a valuable characterisation tool to determine the thermal stability of MOFs,[55] their activation conditions and porosity,[56,57] and it has been widely applied to the quantification of the composition of MOFs.[5,32,34,34,58–62] In fact, the first evidence of defects in MOFs was reported by determining a linker-deficiency by examination of their thermal decomposition profiles.[63] Different methods have been employed to calculate MOF structures based on their thermal degradation profiles,[30,32,63] although it is difficult to find detailed methodology in the literature given the complexity and multifunctionality of the materials, which hinders analysis due to the overlapping

of different decomposition events. A common approach is to compare the theoretical mass decomposition steps for pristine and defective MOF structures to the experimental values to find matching structures.[64,65]Alternative methods calculate the mass per cent corresponding to each decomposition step to calculate the number of linkers and/or modulators,[32,58,63,66] but difficulty increases with multifunctionality and defectivity, with reports often providing qualitative TGA analysis or estimations of MOF composition. In fact, it is common to find comparisons between the experimental and theoretical thermal residues as a validation of MOF composition.

During this manuscript we revise the most common TGA methodology reported in the literature, showing that the TGA-based calculation of MOF composition performed using different methods results in similar trends, but composition values differ depending on the calculation approach, leading to inconsistency in the literature and hindering the high potential of this technique. Hence, we propose new and straightforward TGA methodology, which in combination with the molar ratio of the components – often calculated by other techniques such as Proton Nuclear Magnetic Resonance (^{1}HNMR) analysis for organic components and Inductively coupled plasma mass spectrometry (ICP-MS) or Energy Dispersive X-Ray (EDX) for metals - enables the exact structural determination of almost any MOF structure: pristine and defective MOFs, MTV MOFs, MTVM MOFs, MOFs on MOFs, surface-modified MOFs, MOF composites and loaded MOFs among many other possibilities and combinations of the mentioned examples. It is important to remark that thermal decomposition profiles must be performed under oxidative conditions (air) to achieve full combustion instead of carbonisation of the organic part of the framework and that the nature of the residue (typically metal oxides or salts) has to be identified by other techniques.

Results and discussion

In this manuscript, we will discuss a comprehensive TGA methodology using UiO-66 (UiO stand for University i Oslo)[67] - one of the most greatly studied MOFs - as an example. However, the methodology here discussed can be applied to other MOF systems by changing the MOF structure, the residue, and the charge balance equations accordingly, which will be further detailed. **Figure 1** shows the theoretical thermal decomposition profile of pristine UiO-66 – in which benzene dicarboxylate (BDC) links the metal nodes - alongside its structure at each decomposition step and its mass per cent using the two most common representations of the thermal profiles, either normalising the structure **(method 1)** or the residue **(method 2)** to 100% (See Section S.1 for general remarks, Table S.1), alongside with the equations applied to calculate the composition of MOFs with both literature methods. Although both literature-reported methods can be applied to either normalisation, it is common to see their application as it is exemplified in this publication.

One of the first things to take into account is whether at the time of linker's decomposition - once the MOF has been desolvated, dehydroxylated, dehydrated and modulators have been decomposed, resulting in the (dehydrated) DH MOF - the structure's charge is balanced by oxygen atoms (coming from the decomposition of defect compensating species) as in $\mathbf{Zr_6O_6(L)_xO_{6-x}}$[32] or not as in $\mathbf{Zr_6O_6(L)_x}$.[64] Having found examples of both structures in the literature, we have analysed the theoretical thermal decomposition profiles of $Zr_6O_6(L)_xO_{6-x}$ and $Zr_6O_6(L)_x$ DH MOF theoretical structures with literature-reported and the proposed methodology.

Table 1 shows the MOF and DH MOF structures for a series of pristine and defective MOFs, alongside their theoretical molecular weight, which is used to calculate the mass per cent of the MOF and the DH MOF in the different stages of their thermal decomposition profiles. Calculations of the MOFs composition based on the theoretical decomposition profiles using TGA reported methods (Section S.2 and S.3) are summarised in **Table 2**, in comparison with the method proposed during this manuscript (Section S.4).

We have used the theoretical decomposition profiles of model structures to unequivocally study the mathematical accuracy of the different methods. Proving the methods' precision with TGA traces of synthesised MOFs will be nearly impossible, with only a close estimation using single-crystal characterisation in parallel – modelling solvent in single crystals can be ambiguous, and the measurements are performed from the mother solvent where the crystals grew, differing from the work-up procedures that are used prior to TGA characterisation.

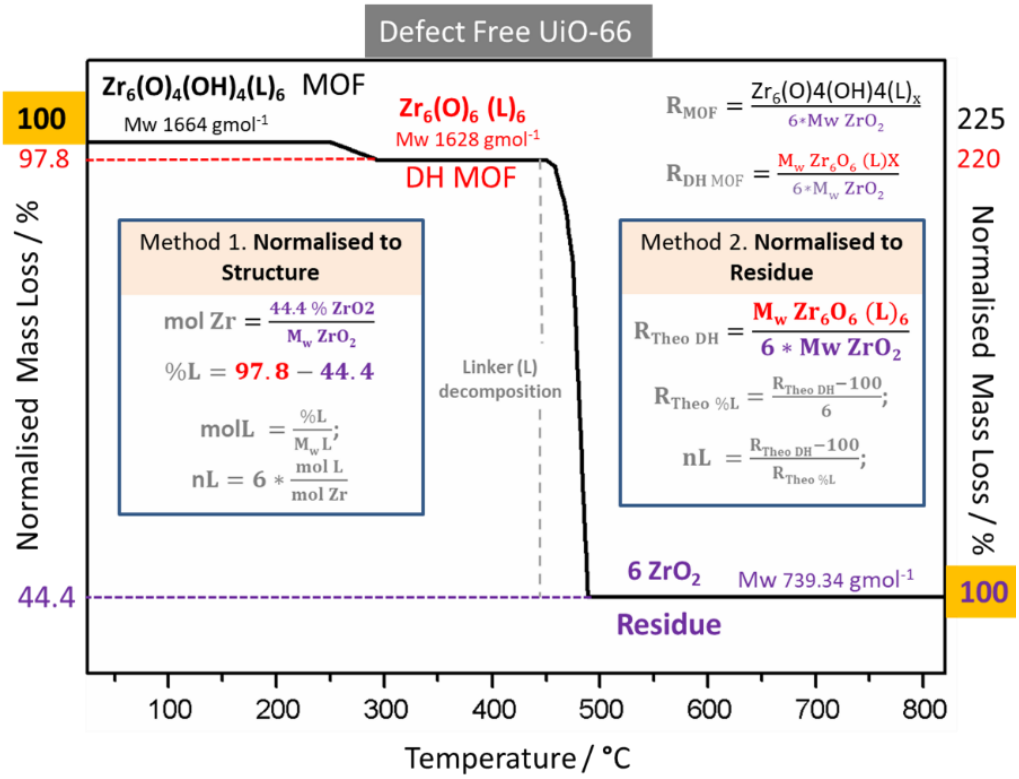

Figure 1: Representation of the theoretical thermal decomposition profiles of pristine UiO-66 (with DH MOFs $Zr_6O_6(L)_xO_{6-x}$), either normalising the MOF structure (left) or the metal residue (right) to 100%, alongside with the TGA calculations based on each literature method.

The elder method for the determination of MOF composition through TGA is detailed on the left-hand side of **Figure 1.** We have used the most commonly reported representation for this method, normalising the start of the decomposition profile to 100% **(method 1**), represented in **Figure 2a**. (S.2. for detailed methodology and calculations).

Table 1: Theoretical pristine and defective UiO-66 structures before and after modulator decomposition and dehydroxylation (DH MOF) with and without charge compensation, alongside with the calculation of their molecular weights that will be used to calculate their theoretical thermal decomposition profiles.

Theoretical Structures					
$Zr_6O_4(OH)_4(L)_X(MOD)_Y$					
MOF	**M_w MOF**	**DH MOF 1**	**M_w DH MOF 1**	**DH MOF2**	**M_w DH MOF 2**
$Zr_6O_4(OH)_4(L)_6$	1664.164	$Zr_6O_6(L)_6$	1628.13	$Zr_6O_6(L)_6$	1628.13
$Zr_6O_4(OH)_4(L)_5(FA)_2$	1590.092	$Zr_6O_6(L)_5(O)_1$	1479.997	$Zr_6O_6(L)_5$	1463.998
$Zr_6O_4(OH)_4(L)_4(FA)_4$	1516.02	$Zr_6O_6(L)_4(O)_2$	1331.864	$Zr_6O_6(L)_4$	1299.866
$Zr_6O_4(OH)_4(L)_3(FA)_6$	1441.948	$Zr_6O_6(L)_3(O)_3$	1183.731	$Zr_6O_6(L)_3$	1135.734
$Zr_6O_4(OH)_4(L)_2(FA)_8$	1277.816	$Zr_6O_6(L)_2(O)_4$	1035.598	$Zr_6O_6(L)_2$	971.602

In method 1 **(Figure 1, Left-hand side)**, the number of moles of the individual components is calculated based on the mass per cent of the structure at each decomposition step. By dividing the moles of linkers by the moles of metal, the linker-metal ratio is obtained, which is then multiplied by the number of metals in the molecular formula. The number of modulators can be calculated by multiplying the number of linkers by the modulator-linker molar ratio (denominated as NMR in further equations) obtained by other techniques, such as ^{1}HNMR (Tables S.2-5).

Shearer *et. al.*[32,58] recently reported a detailed methodology based on the analysis previously reported by Valenzano *et. al*,.[63] represented in the right-hand side of **Figure 1.** To apply this methodology **(method 2)**, the authors normalised the residue to 100%, as represented in **Figure 2b,** which enables the direct comparison of the decomposition steps (S.3. for detailed methodology and calculations).

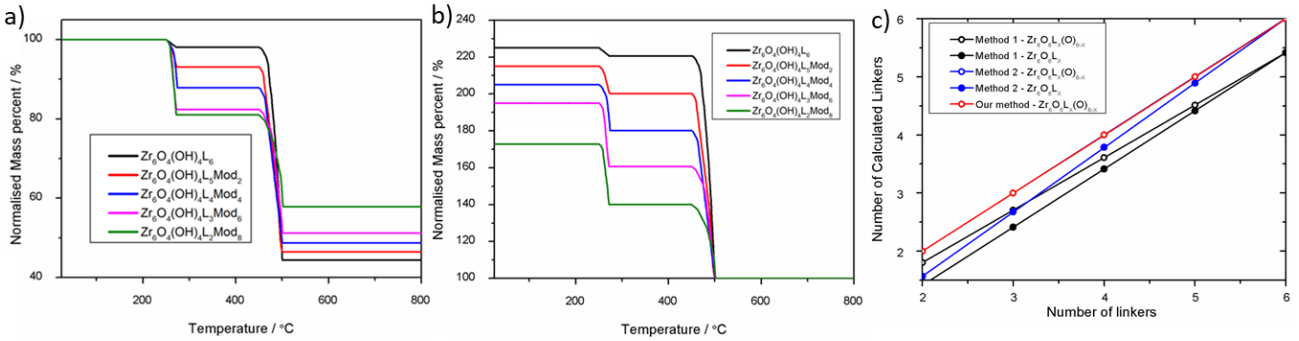

Figure 2: Representation of theoretical thermal decomposition profiles of pristine and defective UiO-66 with DH MOFs Zr6O6(L)xO6-x structures, a) normalising the MOF structure before decomposition to 100% and b) normalising the residue to 100%. d) Representation of the number of calculated linkers with literature reported and our method, using for the decomposition profiles represented in b and c. Method 2 Zr6O6(L)xO6-x matches with our method with minimal error, overlapping in the representation.

In method 2 **(Figure 1, Right-hand side)**, the theoretical mass ratio between the pristine MOF before the linker decomposition step (DH MOF) and its residue, (R_{TheoDH}) is used to calculate the theoretical mass contribution of a linker in the pristine structure ($R_{theor\%\ L}$), which is then used to calculate the number of linkers (nL) in the defective structure. Once the number of linkers has been calculated, the molar ratio between modulator and linker (often calculated by ^{1}HNMR) is used to calculate the number of modulators, providing very close structural determinations (Tables S.6-7).

By looking at the DH MOF structures **(Table 2)** one can notice that the oxygen needed to form the metal oxides that remain in the residue (6 ZrO_2, 12 oxygen atoms) is not accounted in the Zr-Oxo SBU ($Zr_6O_6L_6$ in the pristine structure) and a part of it is taken from the linker carboxylates (one per linker for the pristine structure). This contribution will differ depending on the number of linkers in the structure and on the DH MOF structure (the oxygen contribution from the linker is lower for $\mathbf{Zr_6O_6(L)_x(O)_{6-x}}$ than for $\mathbf{Zr_6O_6(L)_x}$ structures, **Table S.8**). Thus, calculations based on the theoretical thermal decomposition profiles of given structures result in different composition values depending on both the method and on the DH MOF structure, as summarised in **Table 2** and represented **Figure 2c.** The errors are more pronounced if calculations are performed with method 1 (Section S.2) than with method 2 (Section S.3). This is further supported by the fact that subtracting the molecular weight of one oxygen to the molecular weight of the linker results in similar errors to method 2. The new methodology presented in this manuscript (Section S.4) provides exact structural determination for both DH MOF structures due to its mathematic rigour.

Method 2 for $Zr_6O_6(L)_xO_{6-x}$ DH MOFs gives an exact determination of the pristine composition and almost exact determination for defective samples (*ca.* -0.005% error for $Zr_6O_4(OH)_4(L)_5(Mod)_2$ and *ca.* -0.05% error for $Zr_6O_4(OH)_4(L)_2(Mod)_8$) although oxygen compensation is not considered for each specific case during the calculations as such (See Supporting Information for tabulated errors). The calculations are based on the theoretical mass contribution of 1 BDC ($R_{theor\%\ L}$) to the pristine

structure $Zr_6O_6(L)_6$,[32] which is very similar in DH MOF $Zr_6O_6(L)_xO_{6-x}$ defective structures, but in contrast decreases with defectivity in DH MOF $Zr_6O_6(L)_x$ structures (**Table S.8)**, leading to a *ca.* 21.6% error the linker determination for $Zr_6O_4(OH)_4(L)_2(FA)_8$), reinforcing our postulation about the effect of oxygen contribution from the linker to the residue in the calculations (See S.3 for a detailed discussion). This contribution will be more significant for MOF structures in which the defect-free material does not have stoichiometric metal-linker ratios.

Table 2: Structural calculations from theoretical thermal decomposition profiles for given pristine and defective structures. TGA calculations based on the two most common literature methods, for different DH MOF structures (charge-compensated or not), compared to the structural calculations performed with our methodology. (See S.2, S.3 and S.4 for detailed calculations).

Theoretical Structures $Zr_6O_4(OH)_4(L)_X(MOD)_Y$	DH Method 1- 100% MOF				DH Method 2- 100 % Residue				DH Our method	
	$Zr_6O_6(L)_x(O)_{6-x}$		**$Zr_6O_6(L)_x$**		**$Zr_6O_6(L)_x(O)_{6-x}$**		**$Zr_6O_6(L)_x$**		**$Zr_6O_6(L)_x(O)_{6-x}$ or $Zr_6O_6(L)_x$**	
MOF	nL	nMod	nL	nMod	nL	nMod	nL	nMod	nL	nMod
$Zr_6O_4(OH)_4(L)_6$	5.42	0.00	5.42	0.00	6.0000	0.0000	6.0000	0.0000	6.0000	0.0000
$Zr_6O_4(OH)_4(L)_5(FA)_2$	4.51	1.81	4.42	1.77	5.0000	2.0000	4.8920	1.9568	5.0000	2.0000
$Zr_6O_4(OH)_4(L)_4(FA)_4$	3.61	3.61	3.42	3.42	4.0001	4.0001	3.7841	3.7841	4.0000	4.0000
$Zr_6O_4(OH)_4(L)_3(FA)_6$	2.71	5.42	2.42	4.83	3.0001	6.0002	2.6761	5.3522	3.0000	6.0000
$Zr_6O_4(OH)_4(L)_2(FA)_8$	1.81	7.22	1.42	5.66	2.0001	8.0004	1.5681	6.2724	2.0000	8.0000

Since $Zr_6O_6(L)_xO_{6-x}$ neutral structures have been reported in the literature as the DH MOF,[58] both method 2 and method 1 (oxygen-corrected) are appropriate TGA-based structural composition methods that provide an almost exact determination. However, these methods are only possible for MOFs with a clear decomposition of linkers and modulators at different temperatures, since overlapping of the decomposition steps does not allow for the use of the theoretical mass contribution of the linker ($R_{\text{theor\% L}}$) or to accurately calculate the composition of multiple species with method 1 without the oxygen contribution misinterpretation. In fact, detailed TGA determination of UiO-66 structures derived from the modulation with benzoic acid derivatives (which decomposition overlaps with the linker in the MOF structure) is rare in the literature,[66] and the Powder X-Ray Diffraction (PXRD) broad reflection observed as a consequence of the **reo** phase formation is used as an indicator of more defective structures.[68]

Our methodology

Inspired by Valenzano, Shearer *et. al.*,[32,58,63] we have normalised the metal residues of thermal decomposition profiles to 100%, although the method could be applied with either normalisation of the mass weight. Instead of using the theoretical mass contribution of the linker, we have used the **experimental MOF/Residue ratio** (**R_{ExpDH}**), generally expressed as in **Equation 1,** before the linker decomposition step to calculate the MOF's composition.

$$R_{expDH} = \frac{M_w\ [\text{DH structure}]}{M_w\ [\text{Residue}]} = \frac{\text{Mass\% T450°C}}{\text{Mass\% Residue } (=100)}$$

Equation 1: General expression of the experimental ratio between the DH structure, which often decomposes at *ca.* 450 °C, and its residue after thermal decomposition, which is normalised to 100%.

This methodology can also be performed based on the ratio between the structure at the start of the decomposition profiles and its residue (R_{exp}) in combination with the molar ratio of components determined by other characterisation techniques, which avoids incorrect determination as a consequence of the exact determination of the decomposition temperatures (See Section S.4 for detailed calculations).

To simplify calculations with our methodology, we have calculated the structures as a function of the metal (calculating the number of moieties – linker, modulators etc – per metal). This is then multiplied for the number of metals in the molecular formula to obtain the molecular formula unit (Section S.4).

During this manuscript, we propose a multi-faceted TGA methodology for the determination of almost any MOF and MOF composite. Hence, we have classified the thermal decomposition profiles of MOF structures depending on both their composition and the decomposition of their species.

Single MOF species are classified as MOFs composed of one linker, one linker and one or multiple modulators, and multiple linkers and/or modulators**,** which is related to the decomposition temperature of their components: Only linker in the DH MOF (i.e. $Zr_6O_6(L)_xO_{6-x}$) and multiple components in the DH MOF (i.e. $Zr_6O_6(L1)_{6x}(L2)_{6y}(L3)_{6z}O_{6-(6x+6y+6z)}$), which fully or partially decompose during the studied temperature range **(Figure 3)**. MOF composites are classified as MOFs on MOFs or multiple MOF phases, MOFs and inorganic material (i.e. metal oxide or metal nanoparticles), MOFs and organic material (i.e. polymers) and MOFs and hybrid material (i.e. metal complexes), which lead to a classification based on their thermal decomposition extent: 1) inorganic matter which does not thermally decompose, 2) full decomposition of the organic moieties and 3) partial decomposition of organic or hybrid moieties **(Figure 4)**, before, during or after the DH MOF decomposition.

Although we have used derivatives of UiO-66 to exemplify the methodology here proposed, we provide general expression applicable to any defective MOF system and examples of the application of this method to other defective MOF systems - MOF-5,[69] MIL-125 (Materials of Institute Lavoisier),[70] MIL100,[71] HKUST-1 (Hong Kong University of Science and Technology-1)[72] and ZIF-8 (Zeolitic Imidazole Framework-8)[73] – in Section S.4 of the Supporting Information.

Calculation of MOF composition

Thermal degradation profiles of the individual MOF components will provide information about the thermal decomposition steps of the components to identify their degradation temperature and extent. Information provided by other techniques will be needed to determine the molar ratio of the MOF components (introduced as NMR in further equations for simplification) to introduce them as a function of the same variable (for example linker). When multiple modulators and/or linkers are present in the structure, ^{1}HNMR is often a suitable technique to calculate the molar ratio of the components (See S.1 for general remarks), although other techniques such as ICP, UV-Vis or HPLC can be used. A schematic representation of the MOF types and the expression of their R_{exp} and R_{expDH} is given in **Figure 3.**

As MOFs are composed of secondary building units (SBUs) – typically metal-oxo clusters - linked by multidentate ligands, a general example of the calculation of the composition of a defective MOF in which OH^- ligands and modulators compensate the charge arising from missing linkers is given in **Equation 2** (See S.4 for detailed methodology). The combination of the molar ratios between organic components and the charge balance equations, with the experimental ratio between the molecular weight of the structure prior to decomposition and its residue (R_{exp}), results in the exact mathematical determination of the composition.

Including the specifics of a defective MOF system (i.e SBU, linker, modulator and so on) in **Equation 2** leads to the direct determination of its composition avoiding incorrect calculations raising from the incorrect assignment of the different decomposition steps. Note that when monotopic monodentate ligands (such as OH^- or Cl^-) are introduced as defect-compensating ligands for charge balance instead of bidentate monotopic ligands (i.e.monocarboxylates), a paired neutral

molecule (water or solvent) is attached to maintain the coordination number of the metals, (i.e. H_2O/OH^-) pair.

$$R_{exp} = \frac{M_w\left[(SBU)(Linker)_X(Mod)_{Xnmr}(OH/H_2O)_{(SBU\ charge - x(linker\ charge + modulator\ charge * nmr))}\right]}{M_w\,[Metal - oxide\ residue]}$$

$$X\ Linker = \frac{(R_{exp} * M_w\,[Residue]) - M_w\,[SBU] - SBU\ charge * M_w\,[OH/H_2O]}{M_w\,[Linker] + nmr * M_w\,[Mod] - (Linker\ charge + modulator\ charge * nmr) * M_w\,[OH/H_2O]}$$

Equation 2: Expression of the experimental ratio between a defective MOF prior to its decomposition, and its thermal residue. SBU encloses the metal, oxo, hydro, and water molecules. used to calculate the number of linkers in the structure.

An example of the calculation of the number of linkers in a defective UiO-66 MOF compensated by modulators and chlorine, based on its $\mathbf{R_{exp}}$, is given in **Equation 3**. Note that the nature of the defect compensating species will have to be determined by other characterisation techniques such as elemental analysis, ICP, EDX or FT-IR.

$$X\ Ligands = \frac{\left(R_{exp} * M_w\,[ZrO_2]\right) - M_w\ \left[Zr(O)_{\frac{4}{6}}(OH)_{\frac{4}{6}}\right] - 2 * M_w\ [Cl/H_2O]}{M_w\,[L] + NMR * M_w\,[Mod] - (2 + NMR) * M_w\,[Cl/H_2O]}$$

Equation 3: Example of the use of the charge balance equation and the molar ratios to calculate the number of linkers based on the start of the decomposition profile.

If **modulators decompose prior to the DH MOF** structure, the $\mathbf{R_{expDH}}$ is expressed as in **Equation 4,** which is used to calculate the components of the structure. We have performed calculations with $\mathbf{ZrO(L)_xO_{1-x}}$ as the **DH MOF** (Table S.9) but calculations for $ZrO(L)_x$ DH structures for pristine and defective MOFs are also given in Section S.4, (Table S.10), showing also exact structural determination due to the mathematical exactitude of the method. Once the number of linkers per metal (X) has been calculated, the molar ratio between modulator and linker is used to calculate the number of each modulator per metal.[63,66]

$$R_{expDH} = \frac{M_w\,[DH\ MOF]}{M_w\ [Residue]} = \frac{M_w\ [Zr_{6x}O_{6-6x}]}{6 * M_w\ [ZrO_2]} = \frac{M_w\ [ZrO(L)_xO_{1-x}]}{M_w\ [ZrO_2]}$$

$$X\ Ligands = \frac{\left(R_{expDH} * M_w\,[ZrO_2]\right) - M_w\ [ZrO] - M_w\,[O]}{M_w\,[L] - M_w\,[O]}$$

Equation 4: Determination of the number of linkers in MOF structures in which modulators decompose prior to the DH MOF, which is composed of only one linker.

These mathematical principles can be applied to determine the structure of almost any MOF, as summarised in **Figure 3** and Table S.11**,** by changing the MOF structure, its residue and the charge balance equations accordingly in the experimental mass ratios.

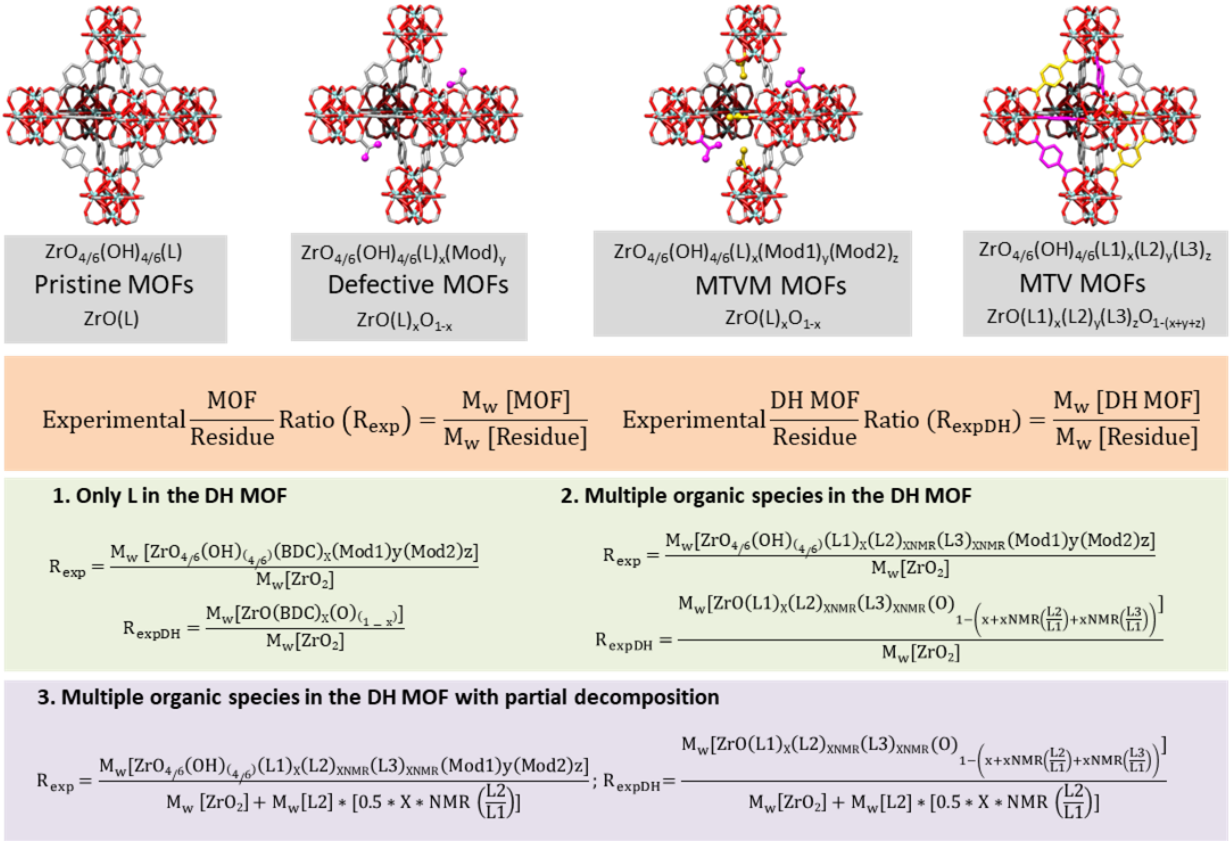

Figure 3: Classification of MOF types depending on their structure composition. Top/Grey: MOF representation alongside with the MOF and DH MOF structure. Orange/Middle: General expressions of the experimental ratio between the MOF structure and its residue (R_{exp}) and between the DH MOF and its residue (R_{expDH}). Green/Middle: TGA methodology for the calculation of the MOFs composition when the linkers fully decompose. Bottom/Blue: TGA methodology for the calculation of MOF structures with multiple linkers, in which one of them partially decomposes.

For example, this methodology can be applied to calculate the composition of DH MOFs with multiple organic species, in which the modulators or surface functionality decomposes during the same temperature range as the linker in the structure, or of MTV MOFs which are composed of multiple linkers (See S.5 for detailed methodology). **Equation 5** exemplifies the calculation of the composition of **MTV MOFs in which the linkers fully decompose together** during the same temperature range. In order to calculate the number of each ligand, the molar ratios (NMR) are used to introduce L2 and L3 as a function of L1. Once L1 (X) has been obtained, the number of L2 and L3 is calculated by multiplying X per the $\frac{L2}{L1}$ and $\frac{L3}{L1}$ NMR molar ratios, respectively. If modulators are also present in the structure, their incorporation can be calculated based on the molar ratios, and the incorporation of other defect compensating species can be calculated by the charge balance equation. Calculations of MTV MOF structures based on their theoretical thermal decomposition profiles – as for defective MOFs – are given in Section S.5 (Tables S.12 and S.13), showing exact structural determination.

$$R_{expDH} = \frac{M_w\ [ZrO(L1)_X(L2)_{XNMR}(L3)_{XNMR}(O)_{1-(XL1+YL2+ZL3)}]}{M_w\ [ZrO_2]}$$

$$x = \frac{\left((R_{expDH} * M_w\ [ZrO_2]) - M_w\,[ZrO] - M_w\,[O]\right)}{\left(M_w\,[L1] + NMR\frac{L2}{L1} * M_w\,[L2] + NMR\frac{L3}{L1} * M_w\,[L3]\right) - \left(1 + NMR\frac{L2}{L1} + NMR\frac{L3}{L1}\right) * M_w\,[O]}$$

Equation 5: Determination of the number of linkers in MTV MOF structures in which the DH MOF's linkers fully decompose during the same temperature range.

If one of the linkers does not fully decompose (**partial decomposition)**, a decomposition ratio can be introduced into the R_{expDH} and/or R_{exp} equations and similar methodology can be applied to obtain the number of each component in the MOF structure (See S.6 for detailed calculations). **Equation 6** shows the calculations based on the general expression of R_{expDH} for an MTV MOF in which one of the linkers decomposition is partial (50%) and Tables S.14 and S.15 show exact compositional determination based on the theoretical thermal decomposition profiles.

$$R_{expDH} = \frac{M_w\ [ZrO(L1)_X(L2)_{XNMR}(L3)_{XNMR}\ (O)_{1-\left(x+xNMR\left(\frac{L2}{L1}\right)+xNMR\left(\frac{L3}{L1}\right)\right)}]}{M_w\ [ZrO_2] + 0.5 * x * NMR\left(\frac{L2}{L1}\right) * M_w\ [L2]}$$

$$x = \frac{\left((R_{expDH} * M_w\ [ZrO_2]) - M_w[\ ZrO] - M_w\ [O]\right)}{\left(M_w\ [L1] + NMR\frac{L2}{L1} * M_w[L2] + NMR\frac{L3}{L1} * M_w[L3]\right) - M_w[O] * \left(1 + NMR\frac{L2}{L1} + NMR\frac{L3}{L1}\right) - M_w[L2] * \left(0.5 * RexpDH * NMR\frac{L2}{L1}\right)}$$

Equation 6: Determination of the number of linkers in MTV MOF structure in which one of the linkers decomposition is partial.

These principles can also be successfully applied to MOFs with multiple decomposition steps (i.e. linkers and/or modulators decomposing at different temperature ranges) using the experimental ratios between the structure at each of the decomposition steps and the residue as in the examples detailed These principles can also be applied to the mass ratio between the structure before its decomposition and the residue.

Calculation of MOF composites

The experimental ratio between the structure and its residue can also be applied to calculate the composition of **MOF composites**. **Figure 4** and Table S.16 summarise the MOF composites to which our TGA methodology is applied during this manuscript, using the same principles described above. The experimental mass ratios (R_{exp} and R_{expDH}) can be generally expressed as a function of the mass fraction of each structure in the MOF composite **(S% Structure)** and as a function of the mass fraction of each structure in the residue of the MOF composite **(R% Structure)**, as in **Equation 7**. Both S% Structure and R% Structure can be calculated from the molar fraction of the components, which can be calculated by various techniques (See S.7 for general remarks and detailed equations of molar and mass fractions). Typically, R% will be used for composites which do not decompose or which decomposition is partial, thus having a contribution to the mass of the residue, while S% is used when R% is not available or when the composite fully decomposes and hence does not contribute to the residue.

If the MOF and the composite are formed of different metals, ICP or EDX can be used to calculate the mass contribution of each of them to the residue (See S.7 for detailed methodology). The individual thermal decomposition profiles of the different MOFs and composites can be used to identify decomposition steps, the residue weight, and the experimental mass ratios of the different components. If the molar ratio of the components is not available through other techniques (i.e. ^{1}HNMR, UV-Vis, ICP-MS, HPLC, FT-IR. EDX etc.) it can be assumed that the MOF is unaltered after the composite formation or inclusion.

$$R_{exp} = \frac{M_w\,[MOF] * S\%MOF + M_w\,[Composite] * S\%Composite}{M_w\,[MOF\ Residue] * S\%MOF + M_w\,[Composite\ Residue] * S\%Composite}$$

$$R_{exp} = \frac{M_w\,[MOF]}{M_w\,[MOF\ Residue]} * R\%MOF + \frac{M_w\,[Composite]}{M_w\,[Composite\ Residue]} * R\%Composite$$

Equation 7: General expression of the experimental ratio between the MOF composite and its residue, which can be used to determine its composition as a function of the mass fraction of a structure in the MOF composite (i.e. S% MOF and S% Comp) and as a function of the mass fraction of each structure in the residue (i.e. R %MOF and R %Comp).

A particular example of MOF composites is the case of **MOFs on MOFs or a mixture of MOF phases.** Their composition can be calculated based on the ratio between the structures and their residue, generally expressed as in **Equation 8,** in combination with other techniques depending on the MOFs' components: different linker and metal (Section S.8.1), different metal same linker (Section S.8.2), and same metal different linker (Section S.8.3).

$$R_{expDH} = \left(\frac{M_w\,[DHMOF1]}{M_w\,[Residue1]} * R\%MOF1\right) + \left(\frac{M_w\,[DHMOF2]}{M_w\,[Residue2]} * R\%MOF2\right)$$

Equation 8: General expression of the experimental ratio between the DH structure of MOF on MOFs composed of different metal and linker.

If the **MOFs** are **composed of different metals and linkers**, knowing the molar ratio between metals (ICP) and between linkers (^{1}HNMR), the mass ratio between the structures and the residue can be expressed as a function of one of the linkers, from which the rest of the components can be determined (See Section S.8.1 for detailed methodology). Tables S.17 and S.18 show that the simultaneous determination of the exact composition of both MOFs is possible with this methodology.

If the species **(metal and/or linker) are the same in both MOF phases** the calculations increase in difficulty, given the number of unknowns in the equation. Isotope labelling and other techniques can be used to identify the molar ratios to be introduced in **Equation 8**. If this is not possible or available to the research team, different assumptions can be introduced into the method, resulting in estimations probably not as close as the exact structural determination. For example, the thermal degradation profile of MOF1 can be used to determine its composition before the growth of MOF2. Introducing MOF1 composition into the MOFs on MOFs R_{expDH} equation can lead to the estimation of the composition of MOF2 (See S.8 for detailed calculations). Tables S.19-21 show that this methodology results in exact compositional determination using the theoretical thermal decomposition profiles of MOF on MOF structures, assuming the structural integrity of the first MOF upon the growth of the second.

To apply this methodology to MOF composites formed of MOF and other material (**Figure 4**), the decomposition of the composing material (further denominated composite for simplification) must be determined. Detailed methodology for all the cases is given in the supporting information, alongside with the pertinent theoretical calculations, showing the exact determination of the MOF composites composition in all cases.

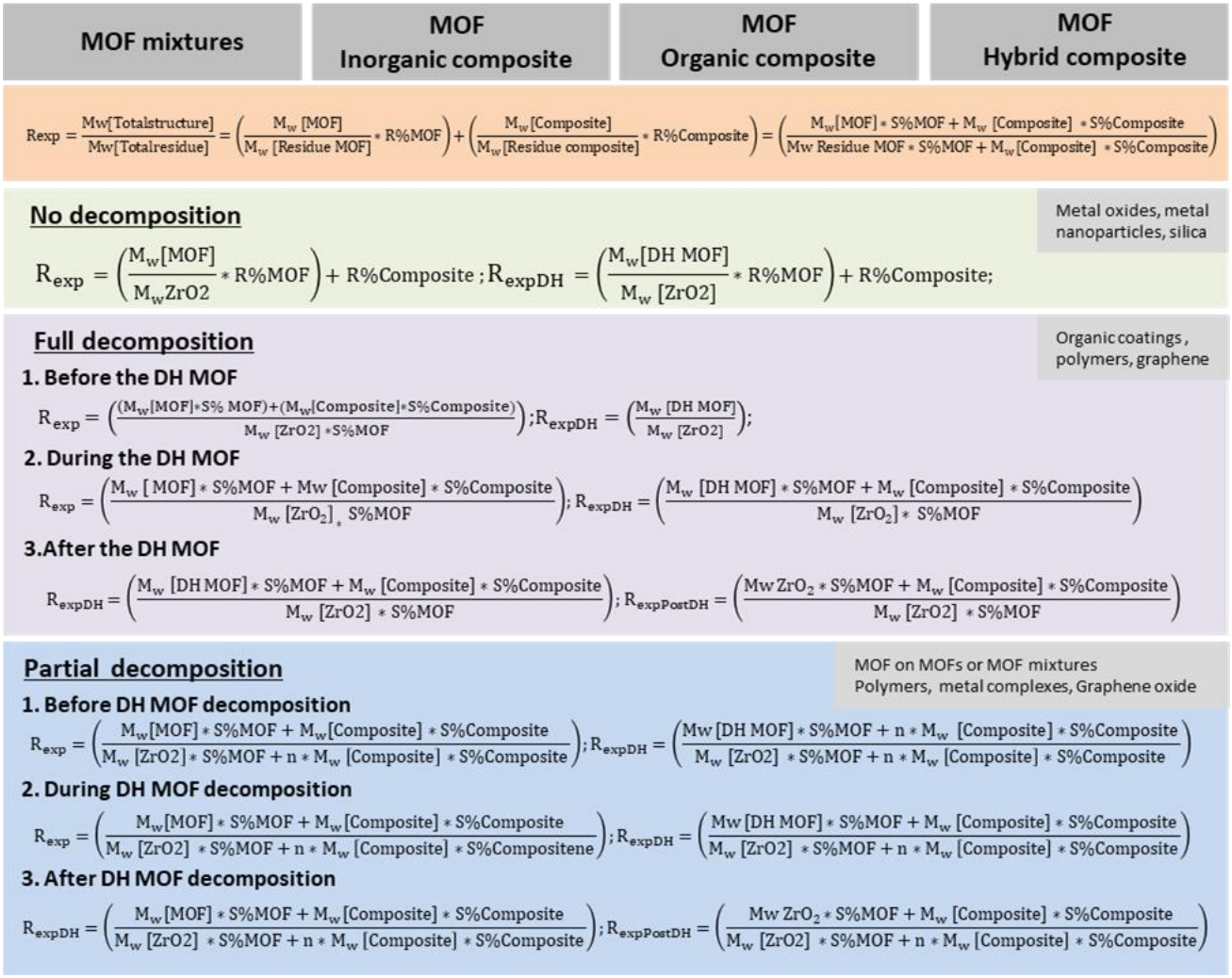

Figure 4: Classification of MOF composites depending on their structure composition. Top/Grey: Types of MOF composites discussed during this manuscript. Orange/Middle: General expressions of the experimental ratio between the MOF composite and its residue (R_{exp}) as a function of the mass fraction of MOF and composite in the structure or the residue. Green/Middle: TGA methodology for the calculation of the MOF composite in which the composite does not decompose. Middle/purple: TGA methodology for the calculation of MOF composite in which the composite fully decomposes. Bottom/Blue: TGA methodology for the calculation of MOF composite in which the composite partially decomposes.

Note that for composites which fully or partially decompose, the expression of the R_{exp} and the calculations derived from it are similar. However, depending on the composite's decomposition temperature, R_{expDH} or $R_{expPostDH}$ can be applied to calculate the mass fraction of composite.

An example of MOF composite in which the composite material **does not decompose** during the temperature ranges studied – typically metal oxides, or metal nanoparticles – is given in **Equation 9** for a TiO_2@UiO-66 MOF composite, (See S.9. for detailed methodology), whereas detailed calculations for theoretical thermal decomposition profiles of TiO_2@UiO-66 defective composites are given in Tables S.22 and S.23, showing exact determination of the composition.

$$R_{exp} = \left(\frac{M_w\,[MOF]}{M_w\,[ZrO_2]} * R\%MOF\right) + (R\%Composite)$$

$$x = \frac{\frac{(R_{exp} - R\%Composite) * M_w[\,ZrO_2]}{R\%MOF} - M_w\left[Zr(O)_{\frac{4}{6}}(OH)_{\frac{4}{6}}\right]}{(M_w\,[L] + NMR * M_w\,[Mod])}$$

Equation 9: Expression of the experimental ratio between MOF composites in which the second material does not decompose and their residue, used to obtain the number of linkers in the MOF structure (x).

If the composite material **fully decomposes prior to the DH MOF decomposition**, since the composite does not contribute to the residue, the R_{expDH} correspond only to the MOF structure, which can be calculated with the methodology previously discussed for MOF systems. The calculated structure can then be introduced into the experimental ratio prior to decomposition (R_{exp}), which can be used to calculate the mass fraction of composite in the structure, as exemplified in **Equation 10** (See S.10.1. for detailed methodology). Detailed structural determination of a series of defective composites where the composite material decomposes before the DH MOF is given in Tables S.24 and S.25, revealing exact compositional determination. If the S% of the composite is known by other techniques, the composition of the MOF can be directly calculated based on the R_{exp}.

$$S\%MOF = \left(\frac{M_w\,[Composite]}{R_{exp} * M_w\,[ZrO_2] - M_w\,[\,MOF] + Mw\,[Composite]}\right)$$

Equation 10: Expression for the calculation of the mass fraction of MOF in a MOF composite in which the second material decomposes prior to the DH MOF.

For a composite that **fully decomposes during the decomposition range of the DH MOF,** the R_{exp} can be expressed as in **Equation 11**. Knowing the mass fraction of the structures (often through ICP), the number of linkers in the DH MOF structure can be determined through calculation of the MOFs molecular weight (See S.10.2 for detailed methodology). Detailed exact determination of the composition of a series MOF composites where the composite material decomposes during the DH MOF is given in Tables S.26 and S.27.

$$R_{exp} = \left(\frac{M_w\,[MOF] * S\%MOF + M_w\,[Composite] * S\%Composite}{M_w\,[ZrO_2] * S\%MOF}\right)$$

$$M_w\,[MOF] = \left(\frac{R_{exp} * M_w\,[ZrO_2] * S\%MOF + M_w[Composite] * S\%Composite}{S\%MOF}\right)$$

Equation 11: Expression of the experimental ratio between MOF composites in which the second material fully decomposes during the DH MOF decomposition, used to obtain the molecular weight of the MOF, from which the molecular structure can be obtained.

If the mass fraction of the material cannot be calculated, the thermal decomposition profiles of the MOF before the composite formation can be used to calculate the MOFs molecular weight - assuming structural integrity upon composite formation – which is used to calculate the mass fraction of composite in the structure, expressed in **Equation 12** (See 10.2 for detailed methodology).

$$SMOF\% = \frac{M_w\ [Composite]}{R_{expDH} * M_w\ [ZrO_2] - M_w\ [DH\ MOF] + M_w\ [Composite]}$$

Equation 12: Expression of the calculation of the mass fraction of a MOF in a MOF composite in which the second material fully decomposes together with the DH MOF, assuming structural integrity of the MOF upon composite formation.

In the case of a composite which **fully decomposes after the DH MOF decomposition** the ratio between the structure after DH MOF decomposition (postDH and the residue can be used to determine the mass fraction of the composite, leading to **Equation 13,** which is then used to calculate the molecular weight of the DH MOF and the subsequent number of linkers through the application of the principles introduced above, (See S.10.3 for detailed methodology). Exact compositional determination of a series of defective MOF composites where the composite material decomposes after to the DH MOF is given in Tables S.28 and S.29.

$$S\%\ MOF = \left(\frac{M_w\ [Composite]}{(R_{expPostDH} - 1) * M_w\ [ZrO_2] + M_w[Composite]}\right)$$

Equation 13: Calculation of the mass fraction of the MOF in a MOF composite in which the composite fully decomposes after the DH MOF.

If the composite material decomposes partially, a decomposition ratio is included in the mass ratios equations as previously described in Section S.6 for MTV MOFs. Although the R_{exp} expression and the approach to calculate the MOF composition based on it will be the same regardless of the decomposition temperature of the composite, methodology based on the R_{expDH} and $R_{expPotDH}$ can be applied to obtain further information depending on the temperature range of decomposition of the species.

The R_{expDH} of a MOF composite in which the **composite material partially decomposes before the DH MOF** decomposition is generally expressed as **Equation 14,** which is used to calculate the molecular weight of the MOF, and subsequently the number of linkers if the mass fraction of the structures is known, as tabulated in Tables S.30 and S.31. The assumption of the structural integrity of the MOF upon the composite formation can be performed to calculate the mass fraction (See S.11.1. for detailed methodology).

$$R_{expDH} = \left(\frac{M_w\ [DH\ MOF] * S\%MOF + n * M_w[Composite] * S\%Composite}{M_w\ [ZrO_2] * S\%MOF + n * M_w\ [Composite] * S\%Composite}\right)$$

$$M_w\ [DH\ MOF] = \left(\frac{R_{expDH} * (M_w\ [ZrO_2] * S\%MOF + n * M_w\ [Composite] * S\%Composite) - n * M_w\ [Composite] * S\%Composite}{S\%MOF}\right)$$

Equation 14: Expression of the experimental mass ratio of MOF composites in which the second material partially decomposes before DH MOF decomposition, used to obtain the molecular weight of the MOF.

For a MOF composite in which the **composite material partially decomposes during the DH MOF** decomposition, the molecular weight of the MOF can be calculated as in **Equation 15,** with similar methodology being used to calculate the number of linkers (Tables S.32 and S.33) or the mass fraction of the structures depending on the information provided by other techniques. (detailed in Section S.11.2).

$$M_w\,[\,MOF] = \left(\frac{R_{exp}*(M_w\,[\,ZrO_2]*S\%MOF+n*M_w\,[Composite]*S\%Composite)-M_w\,[Composite]*S\%Composite}{S\%MOF}\right)$$

Equation 15: Calculation of the molecular weight of the MOF using the expression of the experimental mass ratio between the MOF composite and its residue.

If the composite material partially decomposes after the DH MOF decomposition, the $R_{expPostDH}$ (generally expressed as **Equation 16)** can be used to calculate the mass fraction of the structures, which is then used to calculate the structure of the MOF using the R_{expDH} (detailed in Section S.11.3, Tables S.34 and S.35).

$$R_{expPostDH} = \left(\frac{M_w\,[ZrO_2] * S\%MOF + M_w\,[Composite] * S\%Composite}{M_w\,ZrO_2 * S\%MOF + n * M_w\,[Comp] * S\%Comp}\right)$$

$$S\%Composite = \left(\frac{R_{expPostDH} * M_w\,[\,ZrO_2]-M_w[\,ZrO_2]}{(M_w\,[Composite]-M_w\,[\,ZrO_2])-R_{expPostDH}*n*(M_w\,[Composite]-M_w[\,ZrO_2])}\right)$$

Equation 16: Expression of the experimental ratio between MOF composites in which the second material partially decomposes before DH MOF decomposition, used to obtain the mass fraction of the MOF and subsequently its structure.

Table 3 summarises the approaches used to calculate the composition of different MOF composites depending on the extent of their thermal decomposition (no decomposition, full decomposition and partial decomposition) and their degradation temperature (before, during or after the DH MOF), highlighting the information needed from other techniques to complete the approach, apart from the molar ratio between linkers and modulators. This table shows that less information is needed to calculate the composition of MOF composites when the composite does not decompose or when the decomposition (total or partial) occurs before or after the DH MOF.

Table 3. Methodology applied to calculate the structures of different multicomponent MOF materials, summarising the approach used depending on the information obtained by other techniques, which is underlined after each approach.

MOF COMPOSITE		
Composite with no thermal decomposition: Knowing %R direct MOF structural determination with R_{expDH} (%R)		
Composite with full thermal decomposition		
Before DH MOF	**During DH MOF**	**After DH MOF**
Direct MOF structural determination with R_{expDH}. Then, calculation of S% Composite through R_{exp} (M_w composite)	-Knowing %S direct MOF structural determination with RexpDH ($S\%$ and M_w composite) -Calculation of S% through assumption of MOF integrity through composite formation (M_w MOF, M_w Composite)	Direct determination of S% through $R_{expPostDH}$. Then, direct MOF structural determination with R_{expDH} (M_w composite)
Composite with partial thermal decomposition		
Before DH MOF	**During DH MOF**	**After DH MOF**
-Knowing %R or S% and $R_{expComp}$ direct MOF structural determination with R_{expDH} (R%, Mw composite, $R_{expComp}$) -Calculation of S% through assumption of MOF integrity (M_w MOF, $R_{expComp}$)	-Knowing %R or S% direct MOF structural determination with R_{expDH} (R%, M_w composite, $R_{expComp}$) -Calculation of S% through assumption of MOF integrity through composite formation (M_w MOF, $R_{expComp}$)	Direct determination of S% through $R_{expPostDH}$. Then, direct MOF structural determination with R_{expDH} (M_w composite, $R_{expComp}$)

Conclusions

This comprehensive multi-faceted TGA methodology is an improvement for the characterisation of MOFs, as it enables the determination of the composition of almost any MOF composite based on the analysis of the thermal decomposition profiles, in combination with the molar ratio between components, which can be obtained by other easily accessible characterisation techniques.

Performing an analysis based on the experimental ratio between the structure and its residue enables the exact determination of the number of linkers in any MOF structure without misinterpreting the oxygen contribution from the linkers to the residue. Calculations based on the theoretical thermal decomposition profiles for given samples results in exact structural determination for either of the DH MOF structures analysed, while different composition values are obtained with literature reported methods.

Given the mathematical rigour of the method, the structural composition of MOFs in which multiple organic moieties decompose together with the linker (i.e. modulator, surface functionality, loaded MOFs or MOFs with multiple linkers) can be determined using the mass ratios between structures and residues and the molar ratio between the species.

Going beyond structural complexity and multifunctionality of MOFs, this method also enables the structural determination of MOF composites and we believe that the principles discussed during this manuscript can be applied to virtually almost any MOF material. Additionally, TGA could be coupled to other techniques, such Fourier-Transform Infrared Spectroscopy (FT-IR) or Mass Spectrometry, which in combination with this methodology could provide extensive of knowledge of the composition of MOFs through common and accessible laboratory techniques.

Conflict of interest

The authors have no conflict of interest.

Acknowledgements

This methodology is part of a project that has received funding from the European Union's Horizon 2020 research and innovation programme under the Marie Skłodowska-(grant agreement No 837804, DefTiMOFs, MSCA-IF-2018).

I.A.L thanks the European Union's Horizon 2020 research and innovation programme for the receipt of Marie Skłodowska-Curie Actions Individual Fellowship and The University of Valencia and The Functional Materials Research Team for research facilities.

Sarah L. Griffin is acknowledged by I.A.L for proofreading this manuscript and for meaningful discussion of the methodology here presented. This work would have not been possible without her.

Sergio Tatay Aguilar is acknowledged by I.A.L for the discussion of previously reported TGA methods (denominated method 1 and method 2 in this publication). If the methods we were using did not provide different results, probably this methodology will not have been developed.

IAL thanks Marco Taddei for meaningful discussion and advice.

References

(1) A. Carné-Sánchez, I. Imaz, K. C. Stylianou, D. Maspoch, *Chem. – European. J.*, **2014**, *20*, 5192–5201.

(2) S. Wang, C. M. McGuirk, A. d'Aquino, J. A. Mason, C. A. Mirkin, *Adv. Mater.*, **2018**, *30*, 1800202-1800216.

(3) P. Z. Moghadam, A. Li, S. B. Wiggin, A. Tao, A. G. P. Maloney, P. A. Wood, S. C. Ward, D. Fairen-Jimenez. *Chem Sci*, **2020**, *11*, 2618–2625.

(4) H. Li, M. Eddaoudi, M. O'Keeffe, O. M. Yaghi, *Nature*, **1999**, *402*, 276–279.

(5) I. A. Lázaro, R. S. Forgan *Coordin Chem Rev.*, **2019**, *380*, 230–259.

(6) M. J. Kalmutzki, C. S. Diercks, O. M. Yaghi, *Adv Mater*, **2018**, *30*, 1704304-1704330.

(7) A. U. Czaja, N. Trukhan, U. Müller, *Chem Soc Rev*, **2009**, *38*, 1284-1293.

(8) H. Furukawa, K. E. Cordova, M. O'Keeffe, O. M. Yaghi, *Science.*, **2013**, *341*, 1230444–1230444.

(9) V. Bon, I. Senkovska, S. Kaskel, Green Energy and Technology, **2019**, *55*, 137–172.

(10) . S. Qiu, G. Zhu, *Coord Chem Rev*, **2009**, *253*, 2891–2911.

(11) S. A. A. Razavi, A. Morsali, *Coord Chem Rev*, **2019**, *399*, 213023-213080.

(12) C. V. McGuire, R. S. Forgan, *Chem Comm*, **2015**, *51*, 5199–5217.

(13) R. S. Forgan, *Dalton Trans*, **2019**, *48*, 9037–9042.

(14) Z. Yin, S. Wan, J. Yang, M. Kurmoo, M.-H. Zeng, *Coord Chem Rev*, **2019**, *378*, 500–512.

(15) R. S. Forgan, *Chem Sci* **2020,** *11***,** 4546-4562.

(16) L. Feng, S. Yuan, J.-L. Li, K.-Y. Wang, G. S. Day, P. Zhang, Y. Wang, H.-C. Zhou, *Acs Central Sci*, **2018**, *4*, 1719–1726.

(17) J. Jiao, W. Gong, X. Wu, S. Yang, Y. Cui, *Coordin Chem Rev*, **2019**, *385*, 174–190.

(18) H. Deng, C. J. Doonan, H. Furukawa, R. B. Ferreira, J. Towne, C. B. Knobler, B. Wang, O. M. Yaghi, *Science*, **2010**, *327*, 846–850.

(19) A. M. Rice, G. A. Leith, O. A. Ejegbavwo, E. A. Dolgopolova, N. B. Shustova, *Acs Energy Lett*, **2019**, *4*, 1938–1946.

(20) S. Abednatanzi, P. G. Derakhshandeh, H. Depauw, F.-X. Coudert, H. Vrielinck, P. V. D. Voort, K. Leus, *Chem Soc Rev*, **2019**, *48*, 2535–2565.

(21) K. Koh, A. G. Wong-Foy, A. J. Matzger, *Chem Comm*, **2009**, *41*, 6162-6164.

(22) M. Zhang, D. Wu, Y. Ye, L. Wu, Z. Yao, X. Ma, L. Wang, Z. Zhang, S. Xiang, *Chempluschem* **2018**, *83*, 1044–1051.

(23) T. Li, J. E. Sullivan and N. L. Rosi, *J Am Chem Soc*, **2013**, *135*, 9984–9987.

(24) F. Ke, L.-G. Qiu, Y.-P. Yuan, X. Jiang and J.-F. Zhu, *J Mater Chem*, **2012**, *22*, 9497 -9500.

(25) Y. Peng, M. Zhao, B. Chen, Z. Zhang, Y. Huang, F. Dai, Z. Lai, X. Cui, C. Tan and H. Zhang, *Adv Mater*, **2017**, *30*, 1705454-1705459.

(26) C. Lei, J. Gao, W. Ren, Y. Xie, S. Y. H. Abdalkarim, S. Wang, Q. Ni and J. Yao, *Carbohyd Polym*, **2019**, *205*, 35–41.

(27) T. Rodenas, I. Luz, G. Prieto, B. Seoane, H. Miro, A. Corma, F. Kapteijn, F. X. L. i Xamena and J. Gascon, *Nat Mater*, **2014**, *14*, 48–55.

(28) S. Hermes, T. Witte, T. Hikov, D. Zacher, S. Bahnmüller, G. Langstein, K. Huber and R. A. Fischer, *J Am Chem Soc*, **2007**, *129*, 5324–5325.

(29) H. Guo, Y. Zhu, S. Wang, S. Su, L. Zhou and H. Zhang, *Chem Mater*, **2012**, *24*, 444–450.

(30) L. Yuan, M. Tian, J. Lan, X. Cao, X. Wang, Z. Chai, J. K. Gibson and W. Shi, *Chem Commun*, **2018**, *295*, 469-373.

(31) M. Taddei, K. C. Dümbgen, J. A. van Bokhoven and M. Ranocchiari, *Chem Commun*, **2016**, *52*, 6411–6414.

(32) G. C. Shearer, S. Chavan, S. Bordiga, S. Svelle, U. Olsbye and K. P. Lillerud, *Chemistry of Materials*, **2016**, *28*, 3749-3761.

(33) I. A. Lázaro, C. J. R. Wells and R. S. Forgan, *Angewandte Chemie Int Ed*, **2020**, *59*, 5211–5217.

(34) S. Dissegna, P. Vervoorts, C. L. Hobday, T. Düren, D. Daisenberger, A. J. Smith, R. A. Fischer and G. Kieslich, *J Am Chem Soc*, **2018**, *140*, 11581-11584.

(35) F. Vermoortele, R. Ameloot, L. Alaerts, R. Matthessen, B. Carlier, E. V. R. Fernandez, J. Gascon, F. Kapteijn and D. E. D. Vos, *J Mater Chem*, **2012**, *22*, 10313-10321.

(36) H. Wu, Y. S. Chua, V. Krungleviciute, M. Tyagi, P. Chen, T. Yildirim and W. Zhou, *J Am Chem Soc*, **2013**, *135*, 10525–10532.

(37) O. Kozachuk, I. Luz, F. X. L. i Xamena, H. Noei, M. Kauer, H. B. Albada, E. D. Bloch, B. Marler, Y. Wang, M. Muhler and R. A. Fischer, *Angewandte Chemie Int Ed*, **2014**, *53*, 7058-7062.

(38) K. D. Nguyen, C. Kutzscher, F. Drache, I. Senkovska and S. Kaskel, *Inorg Chem*, **2018**, *57*, 1483–1489.

(39) K. Fan, W.-X. Nie, L.-P. Wang, C.-H. Liao, S.-S. Bao and L.-M. Zheng, *Chemistry-A European Journal*, **2017**, *23*, 6615-6624.

(40) Z. Fang, B. Bueken, D. E. D. Vos and R. A. Fischer, *Angewandte Chemie Int Ed*, **2015**, *54*, 7234-7254.

(41) S. Dissegna, K. Epp, W. R. Heinz, G. Kieslich and R. A. Fischer, *Adv Mater*, **2018**, *10*, 1704501-1704524.

(42) M. Taddei, *Coordin Chem Rev*, **2017**, *343*, 1–24.

(43) M. J. Cliffe, W. Wan, X. Zou, P. A. Chater, A. K. Kleppe, M. G. Tucker, H. Wilhelm, N. P. Funnell, F.-X. Coudert and A. L. Goodwin, *Nat Commun*, **2014**, *5*, 4176-4184.

(44) Y. Liu, R. C. Klet, J. T. Hupp and O. Farha, *Chem Commun*, **2016**, *52*, 7806–7809.

(45) L. Liu, Z. Chen, J. Wang, D. Zhang, Y. Zhu, S. Ling, K.-W. Huang, Y. Belmabkhout, K. Adil, Y. Zhang, B. Slater, M. Eddaoudi and Y. Han, *Nat Chem*, **2019**, *11*, 622–628.

(46) D. Zhang, Y. Zhu, L. Liu, X. Ying, C.-E. Hsiung, R. Sougrat, K. Li and Y. Han, *Science*, **2018**, *359*, 675–679.

(47) L. Zhu, D. Zhang, M. Xue, H. Li and S. Qiu, *CrystEngComm*, **2013**, *15*, 9356-9359.

(48) Q. Li, C. Zhao, X. Chen, W. Wu and Y. Li, *J Anal Appl Pyrol*, **2009**, *85*, 521–528.

(49) Y. K. Du, P. Yang, Z. G. Mou, N. P. Hua and L. Jiang, *J Appl Polym Sci*, **2005**, *99*, 23–26.

(50) Wunderlich, B. *Thermal Analysis of Polymeric Materials*; Springer Science & Business Media, **2005.**

(51) Speyer, R. *Thermal Analysis of Materials*; CRC Press, **1993**.

(52) A. W. Coats and J. P. Redfern, *Analyst*, **1963**, 88, 906-924.

(53) H. Jeske, A. Schirp and F. Cornelius, *Thermochim Acta*, **2012**, *543*, 165–171.

(54) A. A. Jain, A. Mehra and V. V. Ranade, *Fuel*, **2016**, *165*, 490–498.

(55) B. Mu and K. S. Walton, *J Phys Chem C*, **2011**, *115*, 22748–22754.

(56) T. M. McDonald, E. D. Bloch and J. R. Long, *Chem Commun*, **2015**, *51*, 4985–4988.

(57) S. Gadipelli and Z. Guo, *Chem Mater*, **2014**, *26*, 6333–6338.

(58) G. C. Shearer, S. Forselv, S. Chavan, S. Bordiga, K. Mathisen, M. Bjørgen, S. Svelle and K. P. Lillerud, *Top Catal*, **2013**, *56*, 770–782.

(59) F. Vermoortele, B. Bueken, G. L. Bars, B. V. de Voorde, M. Vandichel, K. Houthoofd, A. Vimont, M. Daturi, M. Waroquier, V. V. Speybroeck, C. Kirschhock and D. E. D. Vos, *J Am Chem Soc*, **2013**, *135*, 11465-11468.

(60) W. Liang, L. Li, J. Hou, N. D. Shepherd, T. D. Bennett, D. D'Alessandro and V. Chen, *Chem Sci*, **2018**, *9*, 3508-3516.

(61) R. Wei, C. A. Gaggioli, G. Li, T. Islamoglu, Z. Zhang, P. Yu, O. K. Farha, C. J. Cramer, L. Gagliardi, D. Yang and B. C. Gates, *Chem Mater*, **2019**, *31*, 1655-1663.

(62) Y. Fu, Z. Kang, J. Yin, W. Cao, Y. Tu, Q. Wang and X. Kong, *Nano Lett*, **2019**, *19*, 1618–1624.

(63) L. Valenzano, B. Civalleri, S. Chavan, S. Bordiga, M. H. Nilsen, S. Jakobsen, K. P. Lillerud and C. Lamberti, *Chem Mater*, **2011**, *23*, 1700–1718.

(64) M. J. Katz, Z. J. Brown, Y. J. Colón, P. W. Siu, K. A. Scheidt, R. Q. Snurr, J. T. Hupp and O. K. Farha, *Chem Commun Camb Engl*, **2013**, *49*, 9449–9451.

(65) M. Carboni, C. W. Abney, S. Liu and W. Lin, *Chem Sci*, **2013**, *4*, 2396-2402.

(66) M. Taddei, G. M. Schukraft, M. E. A.Warwick, D. Tiana, M. J. McPherson, D.R. Jones, C. Petit, *J Mater Chem A*, **2019**, 7, 23781-23786.

(67) J. H. Cavka, S. Jakobsen, U. Olsbye, N. Guillou, C. Lamberti, S. Bordiga and K. P. Lillerud, *J Am Chem Soc*, **2008**, *130*, 13850–13851.

(68) C. Atzori, G. C. Shearer, L. Maschio, B. Civalleri, F. Bonino, C. Lamberti, S. Svelle, K. P. Lillerud and S. Bordiga, *J Phys Chem C*, **2017**, *121*, 9312–9324.

(69) H. Li, M. Eddaoudi, H. Li, M., O' Keeffe, M. and Yaghi, O. M., *Nature*, **1999**, *402*, 276-279.

(70) M. Dan-Hardi, C. Serre, T. Frot, L. Rozes, G. Maurin, C. Sanchez, G.A Férey, *J. Am Chem Soc*, **2009**, *131*, 10857–10859.

(71) J. Castells-Gil, N. M. Padial, N. Almora-Barrios, I. da Silva; D. Mateo, J. Albero, H. García, C. Martí-Gastaldo, *Chem Sci*, **2019**, *10*, 4313-4321.

(72) S. S. Y. Chui, S. M. F. Lo, J. P. H. Charmant, A. G. Orpen, I. D. Williams, *Science*, **1999**, *283*, 1148-1150.

(73) A. Phan, C. J. Doonan, F. J. Uribe-Romo, C. B. Knobler, M. O'Keeffe, O. M. Yaghi, *Acc. Chem Res*, **2010**, *43*, 58–67.